Implications for Solar Neutrino Oscillations from Super-Kamiokande and SNO Data

Michael B. Smy

Department of Physics & Astronomy, 4182 Frederick Reines Hall, University of California, Irvine Irvine, California 92697-4575, USA

E-mail: smy@solar1.ps.uci.edu

ABSTRACT

Super-Kamiokande uses neutrino-electron elastic scattering to measure the recoil electron spectrum and zenith-angle dependence of solar ^{8}B neutrinos. SNO has measured the ^{8}B neutrino–deuteron charged-current reaction rate. The elastic scattering rate, spectrum and zenith-angle dependence in conjunction with the charged-current reaction rate favors active neutrino oscillations at large mixing angles by about 3σ over the no-oscillation hypothesis and small mixing angles. The analysis is independent of the absolute ^{8}B and *hep* flux and assumes two-flavor oscillations described by mixing angle and mass^2 difference. Two allowed regions at large mixing are found.

1. Introduction

A simple two-neutrino oscillation model ($\nu_e \longrightarrow \nu_x$) is capable of explaining why all rates measured by various solar neutrino experiments[1,2,3,4,5,6] are smaller than predictions based on the standard solar model[7]. Elastic neutrino-electron scattering is sensitive to all active neutrino types. However, the cross section for muon- or tau-type neutrinos is about 5.2 to 6.8 times smaller than for electron-type neutrinos. The neutrino–deuteron charged-current reaction on the other hand only measures the electron-type neutrino flux. Neutrino flavor oscillation into muon- or tau-type will suppress the observed charged-current reaction rate more strongly than the observed elastic scattering rate. A combined fit to the elastic scattering precision data of Super-Kamiokande[5] and SNO's measurement of the charged-current reaction rate[6] can therefore indicate active neutrino oscillations. Since both experiments measure the solar neutrino flux from the ^{8}B branch of the solar neutrino spectrum, the results of such a combined fit are independent of solar neutrino flux predictions by the standard solar model. In addition to this comparison between the rates of Super-Kamiokande and SNO, the shape of Super-Kamiokande's recoil electron spectrum and its data on the zenith-angle dependence of the solar neutrino flux constrain[8] the mixing angle θ and mass^2 difference Δm^2 between the two neutrinos.

The solar neutrino rate measurements also define allowed areas for these parameters. The mixing angle of the large mixing angle solution is close to maximal (around $\sin^2 2\theta \approx 0.8$) and has a range in Δm^2 of $8 \cdot 10^{-6}\mathrm{eV}^2$ to $3 \cdot 10^{-4}\mathrm{eV}^2$. The mixing angle of the small mixing angle solution is between $2 \cdot 10^{-3}$ and 10^{-2} for a Δm^2 between $4 \cdot 10^{-6}\mathrm{eV}^2$ and $10^{-5}\mathrm{eV}^2$. The low solution is at maximal mixing between $6 \cdot 10^{-8}\mathrm{eV}^2$

and $2{\cdot}10^{-7}\mathrm{eV}^2$. Vacuum solutions occur between $6{\cdot}10^{-11}\mathrm{eV}^2$ and $10^{-10}\mathrm{eV}^2$ for mixing angles above $\sin^2 2\theta > 0.5$ and some quasi vacuum solutions (with lower probability) between $2 \cdot 10^{-10}\mathrm{eV}^2$ and $7 \cdot 10^{-10}\mathrm{eV}^2$ at maximum mixing.

2. Analysis Method

The oscillation analysis is similar to the analysis of the Super-Kamiokande zenith angle spectrum [8]. For each energy bin i, we form a zenith angle rate difference vector $\overrightarrow{\Delta_i}$. Its seven zenith components $\Delta_{i,z}$ are

$$\Delta_{i,z}(\sin^2 2\theta, \Delta m^2; \alpha, r_{hep}) = \frac{\phi_{i,z}^{\mathrm{meas}}}{\phi_i^{\mathrm{SSM}}} - \alpha \times f\,(E_i, \delta_{\mathrm{corr}}) \times \frac{\phi_{i,z}^{\mathrm{osc}}(\sin^2 2\theta, \Delta m^2; r_{hep})}{\phi_i^{\mathrm{SSM}}}$$

where θ is the two-neutrino mixing angle and Δm^2 the mass^2 difference between the neutrinos. The parameter α normalizes the neutrino flux and r_{hep} describes the *hep* flux relative to the ^{8}B flux. The observed rate in energy bin i and zenith angle bin z is denoted as $\phi_{i,z}^{\mathrm{meas}}$; ϕ_i^{SSM} and $\phi_{i,z}^{\mathrm{osc}}$ (calculated as in[8]) are the expected event rates in that bin without and with neutrino oscillation. The spectral distortion f due to the correlated systematic error of $\phi_{i,z}$ is scaled by the parameter δ_{corr}. Similarly, we define the charged-current rate difference

$$\Delta_{\mathrm{CC}}(\sin^2 2\theta, \Delta m^2; \alpha, r_{hep}) = \frac{\phi_{\mathrm{CC}}^{\mathrm{meas}}}{\phi_{\mathrm{CC}}^{\mathrm{SSM}}} - \alpha \times \frac{\phi_{\mathrm{CC}}^{\mathrm{osc}}(\sin^2 2\theta, \Delta m^2; r_{hep})}{\phi_{\mathrm{CC}}^{\mathrm{SSM}}}.$$

To compute $\phi_{\mathrm{CC}}^{\mathrm{osc}}$ the neutrino–deuteron charged-current cross section calculation of Ying, Haxton and Henley[9] is used. The oscillation probability is calculated in a similar way as for $\phi_{i,z}^{\mathrm{osc}}$. The χ^2 is defined as

$$\chi^2(\sin^2 2\theta, \Delta m^2) = \min_{\alpha, r_{hep}} \left(\sum_{i=1}^{8} \overrightarrow{\Delta_i} \cdot V_i^{-1} \cdot \overrightarrow{\Delta_i} + \left(\frac{\delta_{\mathrm{corr}}}{\sigma_{\mathrm{corr}}}\right)^2 + \left(\frac{\Delta_{\mathrm{CC}}}{\sigma_{\mathrm{CC–ES}}}\right)^2 \right) \qquad (1)$$

Each energy bin i has a separate $7{\times}7$ error matrix V_i describing the energy-uncorrelated uncertainty. V_i is the sum of the statistical error matrix and the energy-uncorrelated systematic error matrix, the latter of which is constructed assuming full correlation in zenith angle. The flux normalization factor α is constrained by the last term containing the uncertainty $\sigma_{\mathrm{CC–ES}}$. This uncertainty is the quadratic sum of SNO's statistical and systematic uncertainty and the systematic uncertainty of Super-Kamiokande's total rate. It is the systematic uncertainty of the SK–SNO rate difference combined with the SNO statistical uncertainty.

3. Results of the χ^2 Analysis

Active two-neutrino oscillations are favored by 3σ over the no-oscillation hypothesis. The allowed parameter regions are shown in figure 1 (logarithmic scale for $\sin^2 2\theta$)

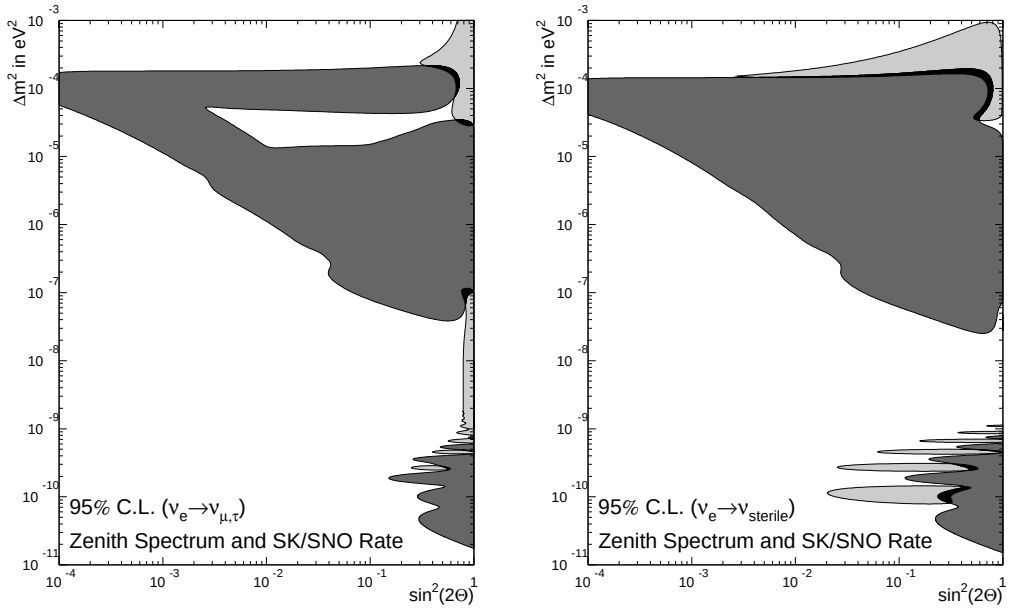

Figure 1: Excluded regions (dark shaded area; 95% C.L.) using the shape of the zenith angle spectrum[8] and allowed regions (light shaded area; 95% C.L.) using the rate and zenith angle spectrum and the charged-current reaction rate for fully active (left) and fully sterile (right) two-neutrino oscillations.

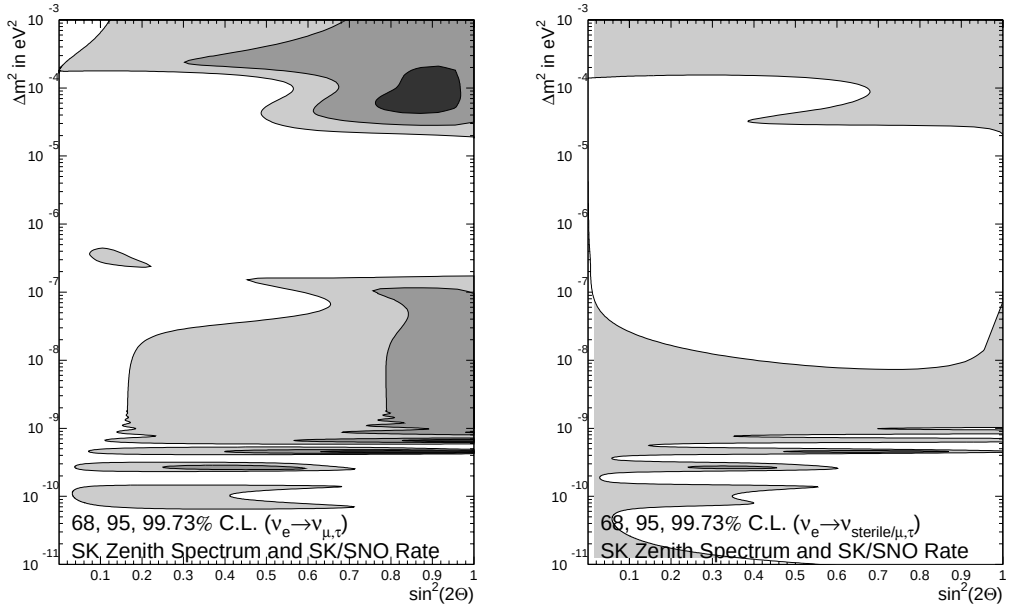

Figure 2: Allowed regions using the shape of the zenith angle spectrum and allowed regions at the one (dark shaded area), two (shaded area) and three (light shaded area) sigma level using the rate and zenith angle spectrum and the charged-current reaction rate for fully active (two neutrinos; left) and fully sterile (three neutrinos; right) oscillations. The horizontal scale is linear.

and figure 2 (linear scale). The best fit is at $\Delta m^2 = 6.6 \cdot 10^{-10}\mathrm{eV}^2$ and maximal mixing. The χ^2 is 37.9 with 41 degrees of freedom (44 variables from the Super-Kamiokande zenith angle spectrum, one from the SNO rate; four parameters are minimized). The best-fit ^{8}B flux is 78% of the standard solar model prediction, the best-fit *hep* flux is zero. The allowed areas in figure 1 for the sterile case are based on a two-neutrino oscillation analysis with two parameters ($\sin^2 2\theta$ and Δm^2) and a minimum in the sterile vacuum region. This χ^2 minimum is worse by 6.4 compared to the best-fit active solution. A one parameter (sterile content of the oscillation regardless of $\sin^2 2\theta$ and Δm^2) interpretation of this χ^2 difference implies that fully sterile oscillations (sterile content=1) are disfavored by more than 2.5σ compared with fully active two-neutrino oscillations (sterile content=0). The sterile case of figure 2 uses the sterile content of the oscillation as a third parameter and the best-fit active oscillation solution as the minimum. The small mixing angle solution is disfavored in both the fully active and the fully sterile case.

Figure 3 shows the best-fit charged-current rate (to be compared directly with the SNO measurement). Figure 4 displays the best-fit ^{8}B flux in units of the standard solar model prediction. In case of the active large mixing angle and low solutions, the best-fit ^{8}B agrees with the prediction within the theoretical uncertainty. Only some active quasi-vacuum solutions disagree by more than 2σ from the prediction. The allowed areas shown in the sterile case use the best-fit sterile solution (disfavored by $> 2.5\sigma$) as the minimum. In general, agreement of the best-fit ^{8}B flux with the prediction is poor in those areas. In some parts of a 'sterile large mixing angle solution', however, the ^{8}B flux agrees well.

Allowed areas are near the active large mixing angle solution and a band at maximum mixing extending from the low solution down to the quasi-vacuum region. Figure 3 shows the reason why the small mixing angle solutions and most of the vacuum solutions are disfavored. The best-fit charged-current rate is in agreement with the SNO measurement mostly in those areas that disagree with the Super-Kamiokande zenith angle spectrum. In the active case, only the upper part of the large mixing angle solution and a small band extending from the low to the quasi vacuum solution are outside the Super-Kamiokande excluded area *and* lead to an acceptable fit of the SNO rate.

In the sterile case, no good agreement is found outside the Super-Kamiokande excluded area. In particular, active small mixing angles are disfavored since they either show spectral distortions and core enhancement (and disagree with the Super-Kamiokande spectrum) or have large electron-type survival probabilities. In the latter case, the flux difference between Super-Kamiokande and SNO cannot be explained. The best fit close to the small mixing angle solution (see light grey lines and band on the left-hand side of figure 5) has almost no spectral distortion and a survival probability around 90%. This is due to the very small mixing angle ($\sin^2 2\theta < 10^{-3}$). The contribution of muon- or tau-type neutrinos to the SK rate (see difference between

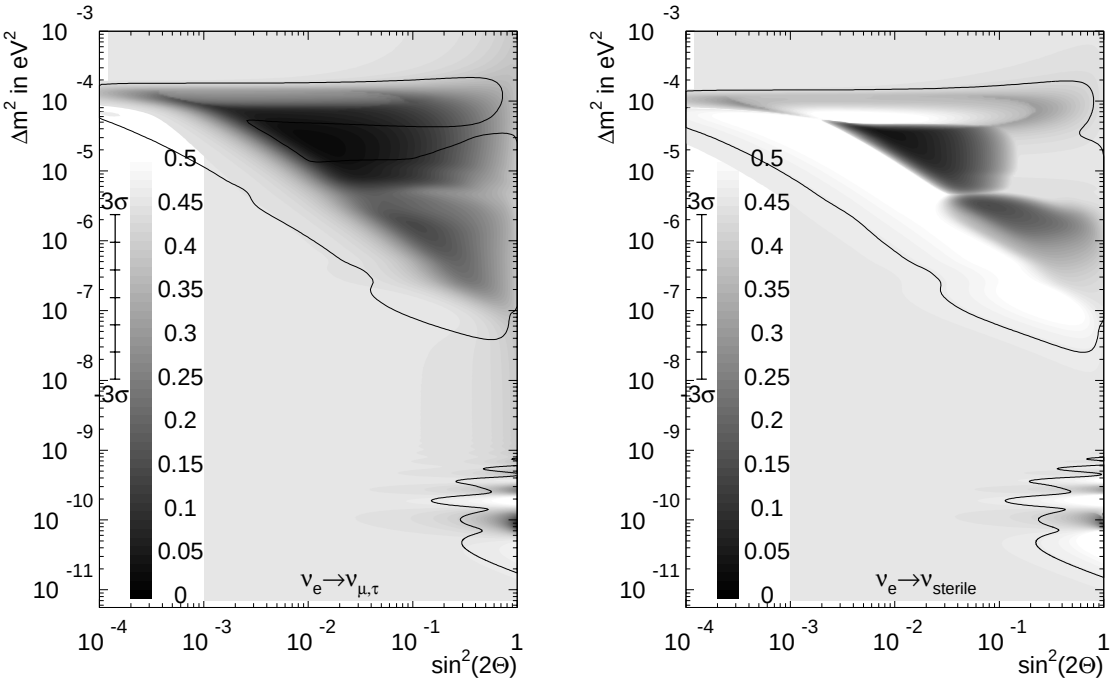

Figure 3: Best-fit charged-current rate in SNO as a function of mixing and mass^2 difference for fully active (left) and fully sterile (right) two-neutrino oscillations. The black lines enclose the area excluded by the shape of the Super-Kamiokande zenith angle spectrum[8)] at 95% C.L.

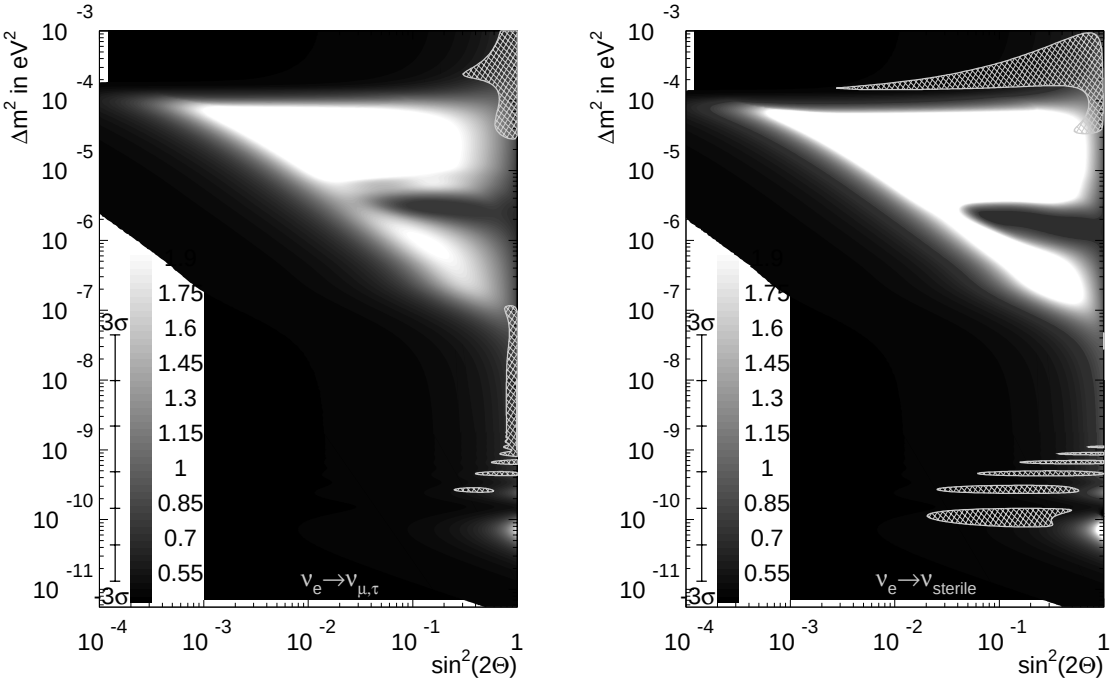

Figure 4: Best-fit ^8B flux in units of the standard solar model prediction as a function of mixing and mass^2 difference for fully active (left) and fully sterile (right) two-neutrino oscillations. The hatched areas are allowed at 95% C.L. by the Super-Kamiokande zenith angle spectrum and the Super-Kamiokande–SNO rate comparison.

dashed and solid line) is very small; the SK and SNO rates are predicted to be very similar. Since the survival probability is so large, the ^{8}B flux is only about 50% of the standard solar model prediction.

The best-fit large mixing angle solution (dark grey lines and band in the left-hand side of figure 5) on the other hand can reconcile the flat spectrum and a low survival probability (around 35%). Large mixing angle solutions with strong day-night asymmetries are disallowed by the Super-Kamiokande zenith angle distribution. At present, SNO data does not have enough precision to observe the weaker day-night asymmetry predicted by the best-fit large mixing angle solution (see dark grey lines and band in figure 6). The ^{8}B flux agrees with the standard solar model prediction. The best-fit *hep* flux is about 2.7 times larger than predicted. Note that all displayed spectrum predictions in figures 5 and 6 assume the standard solar model *hep* flux.

The quasi vacuum solution (dark grey lines and band in the right-hand side of figure 5) follows best the shape of the spectrum. The survival probability of about 47% is just small enough to accommodate the SK–SNO rate difference within systematic uncertainty, assuming the ^{8}B flux is about 1.2σ below the standard solar model value. The best-fit *hep* flux is zero.

The spectrum of the low solution (light grey lines and band in the right-hand side of figure 5) fits somewhat worse than the spectrum of the large mixing angle solution. It is also disfavored by its zenith angle variation (see light grey lines and band in figure 6). A survival probability of about 45% accommodates the SK–SNO rate difference within systematic uncertainty. The ^{8}B flux is about 1 standard deviation below the standard solar model prediction, the best-fit *hep* flux is twice as large as in the standard solar model.

4. Conclusions

Combining Super-Kamiokande and SNO solar neutrino data places strong constraints on solar neutrino oscillations independently of standard solar model neutrino flux predictions. Large mixing angle active oscillation solutions are favored by about 3σ over small mixing angles. Fully sterile oscillations are disfavored by more than 2.5σ. Two allowed areas (one above $\Delta m^2 = 3 \cdot 10^{-5}\mathrm{eV}^2$ and one below $\Delta m^2 = 10^{-7}\mathrm{eV}^2$) are found. For most active solutions, the best-fit ^{8}B flux agrees with the standard solar model prediction within the given uncertainty. For most sterile solution, the best-fit ^{8}B flux does not agree well with the standard solar model prediction. The electron-type survival probability for ^{8}B neutrinos is expected to be between 30% and 47%. Spectral distortions and zenith angle variations should also be small for ^{8}B neutrinos.

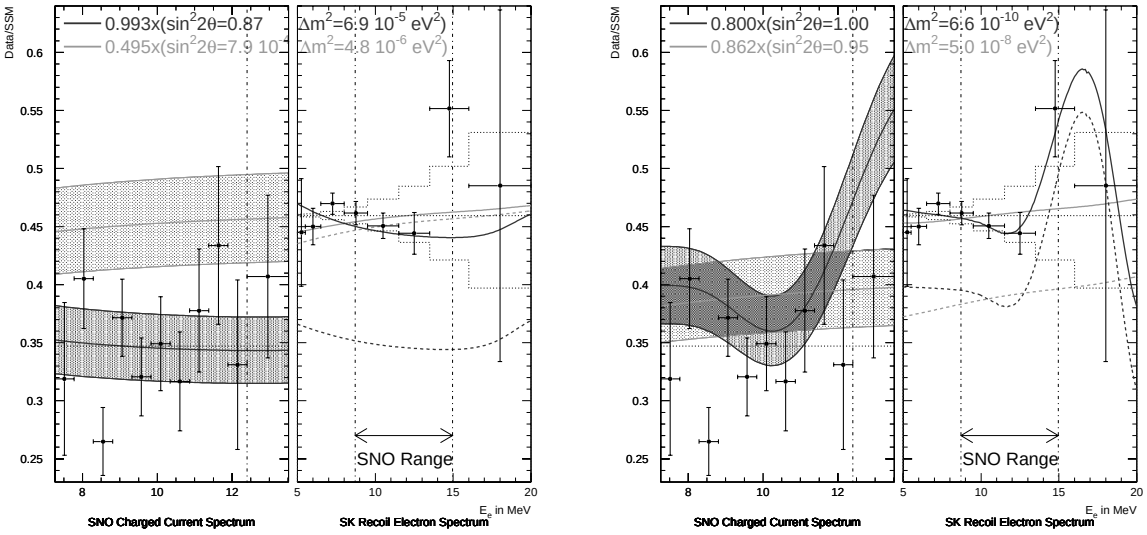

Figure 5: SNO Spectrum (left panel) and SK Spectrum (right panel) compared with the best-fit large mixing angle (left figure; dark grey), small mixing angle (left figure; light grey), low (right figure; light grey) and vacuum (right figure; dark grey) solution predictions. The bands around the SNO predictions indicate the systematic uncertainty for the SK—SNO flux difference. The dashed lines below the SK predictions are the contributions due to electron-type neutrinos only. The dotted histograms show the $\pm 1\sigma$ systematic energy-correlated uncertainty.

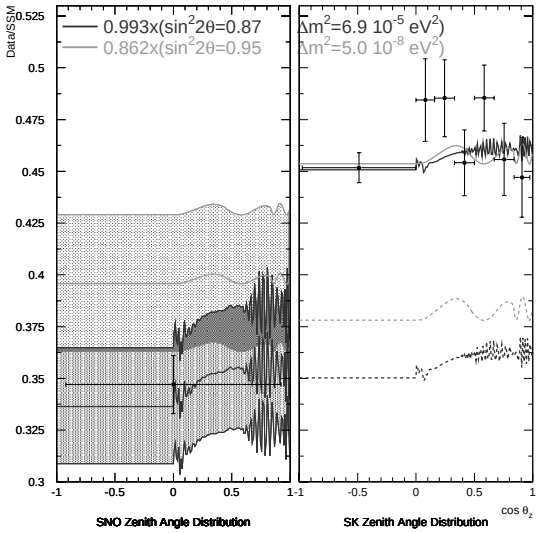

Figure 6: Zenith Angle Distribution for SNO (left panel) and SK (right panel) compared with the best-fit large mixing angle (dark grey) and low solution (light grey) predictions.

5. Acknowledgements

The author acknowledges the cooperation of the Kamioka Mining and Smelting Company. The Super-Kamiokande detector has been built and operated from funding by the Japanese Ministry of Education, Culture, Sports, Science and Technology, the U.S. Department of Energy, and the U.S. National Science Foundation.

6. References

1) B. T. Cleveland et al. *Astrophys. J.* **496** (1998) 505.
2) Kamiokande Collaboration, Y. Fukuda et al., *Phys.Rev.Lett.* **77** (1996) 1683.
3) V. Gavrin, *Nucl. Phys. B(Proc. Suppl.)* **91** (2001) 36;
J. N. Abdurashitov et al., *Phys. Lett. B***328** (1994) 234.
4) E. Bellotti, *Nucl. Phys. B(Proc. Suppl.)* **91** (2001) 44;
W. Hampel et al., *Phys. Lett. B***388** (1996) 364;
P. Anselmann et al., *Phys. Lett. B***342** (1995) 440.
5) Super–Kamiokande Collaboration, S. Fukuda et al. *Phys.Rev.Lett.* **86** (2001) 5651-5655.
6) SNO Collaboration, Q. R. Ahmad et al., *nucl-ex/0106015*, submitted to *Phys.Rev.Lett.*.
7) J. N. Bahcall et al., *astro-ph/0010346*.
8) Super–Kamiokande Collaboration, S. Fukuda et al. *Phys.Rev.Lett.* **86** (2001) 5656-5660.
For additional details, see also *hep-ex/0106064*, to be published in proceedings of XXXVIth Rencontres de Moriond on Electroweak Interactions and Unified Theories.
9) S. Ying, W. C. Haxton, E.M. Henley, *Phys.Rev.* **C45** (1992) 1982-1987.
See also J. N. Bahcall and E. Lisi, *Phys. Rev.* **D54** (1996) 5417.